sciendo
ISSN 1335-8871
MEASUREMENT SCIENCE REVIEW
Journal homepage: https://content.sciendo.com

The Collection Efficiency of a Large Area PMT Based on the Coated MCPs

Xingchao Wang[1,3], Lin Chen[2], Qilong Wang[1], Jianli He[5], li Liping Tian[2], Jinshou Tian[4], Lingbin Shen[2], Yunji Wang[2]

[1]*School of Electronic Science and Engineering, Southeast University, Nanjing 210096, China*
[2]*School of network and communication engineering, Jinling Institute of Technology, Nanjing 211169, China,* chenlin_7474@163.com
[3]*North Night Vision Technology (NNVT) CO., LTD, Nanjing 210110, China*
[4]*State Key Laboratory of Transient Optics and Photonics, Xi'an Institute of Optics and Precision Mechanics (XIOPM), Chinese Academy of Sciences (CAS), Xi'an 710119, China,* tianjs@opt.ac.cn
[5]*Inner Mongolia University of Science and technology, Baotou 014010, China*

Abstract: The electron collection efficiency (*CE*) of the photomultiplier tube based on microchannel plates (MCP-PMT) is limited by the MCP open area fraction. Coating MCP with a high secondary yield material is supposed to be an effective approach to improve *CE*. Both typical and coated MCP-PMTs are developed. A relative measurement method is proposed to characterize the collection efficiency performance. Results show that the PMT based on the coated MCPs has a significant improvement on *CE*, a good gain uniformity and a high precise energy resolution.

Keywords: Photomultiplier tube, Microchannel plate, Collection efficiency.

1. INTRODUCTION

Jiangmen Underground Neutrino Observatory (JUNO) [1]-[6] was proposed as the Daya Bay [7]-[9] II in 2012. The energy resolution was required to be $3\%\sqrt{E(MeV)}$, which means that the detection efficiency (*DE*) of the 20-in. photomultiplier tube (PMT) should be above 25 %. At that time, none of the 20-in. PMT products could meet this criterion. In this situation, the 20-in. large area PMT based on the microchannel plates (MCP-PMT) [10], [11] was proposed and developed by the MCP-PMT collaboration formed by the scientists from the Institute of High Energy Physics (IHEP) of the Chinese Academy of Sciences, Northern Night Vision Technology Co., LTD (NNVT) and the Xi'an Institute of Optics and Precision Mechanics (XIOPM) of the Chinese Academy of Sciences.

The 20-inch MCP-PMT prototype is shown in Fig.1. It is well known that *DE* is the product of quantum efficiency (*QE*) and collection efficiency (*CE*) [12]. To obtain a high *DE*, *QE* and *CE* should be fairly high. For the high *QE* performance, transmission and reflection photocathode layers are deposited on the inner face of the upper and lower semi-ellipsoidal glass shell, respectively.

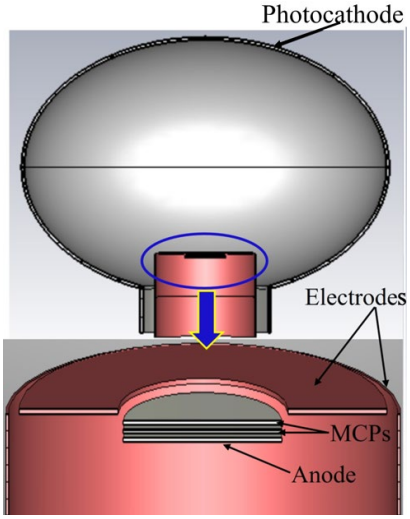

Fig.1. Schematic diagram of the 20-inch MCP-PMT.

CE is another crucial parameter. In the 20-inch MCP-PMT, a pair of "V" stacked MCPs is adopted to displace the conventional discrete dynodes. Compared to the dynodes, MCPs offer some outstanding features, such as high gain, fast time response, stable operation even in high magnetic fields,

DOI: 10.2478/msr-2022-0030

low power consumption, and easy assembly. In the early MCP-PMT samples, MCP is uncoated. The flat inter-channel area on the MCP input face is a nickel-chromium (Ni-Cr) electrode which has a maximum secondary electron yield (SEY) at typical incidence

$$(\delta_e)_{max} \approx 1 \tag{1}$$

for primary energy $E \approx 500$ eV [13]. Photoelectrons striking at the Ni-Cr have a strong possibility of being absorbed without emission. Accordingly, *CE* of the early MCP-PMT is limited by the MCP open area fraction (A_{open}) [14]. Considering secondary electron emission phenomenon on the MCP input electrode, the contribution of electrons to the MCP-PMT collection efficiency can be divided into two parts. One of them is represented by the photoelectrons entering the channel entrances directly, which is referred to as the primary electron contribution CE_p. The other part consists of generations of secondaries (excited by electrons striking the MCP input electrode) entering the channel entrances by an appropriate-directed electric field, which is referred to as the secondary electron contribution CE_s. It is evident that CE_p is never greater than A_{open}. The only approach to make *CE* a significant improvement is to improve CE_s. Accordingly, plating a high SEY material on the first MCP in the MCP-PMT is proposed [15], [16]. A great deal of secondaries can be excited by the photoelectrons impacting the MCP coated electrode and be collected by MCP channels. This approach has already been validated by the simulation [15], [16]. However, it has not been validated by any experiments.

In this paper, the 20-inch typical and coated MCP-PMT samples are developed. Experiments are conducted to systematically investigate their performances.

2. Experiment procedures & results

The 20-inch coated MCP-PMT samples (shown in Fig.2.) including the transmission-reflection photocathode, two focusing electrodes and a pair of "V" stacked coated MCPs are developed in XIOPM lab to validate the effectiveness of this approach. The collection efficiencies CE_s of the typical and coated MCP-PMTs are investigated by the experiments. A relative measurement method is developed to characterize their performances. As mentioned above, *CE* is expressed as a ratio of *DE* to *QE*. In our experiments, the illuminated point on the photocathode corresponding to the maximum collection efficiency (CE_{max}) is chosen as a reference. The relative collection efficiency (CE_r) for other illuminated points is expressed as

$$CE_r = \frac{CE}{CE_{max}} = \frac{\frac{DE}{QE}}{\frac{DE_{max}}{QE_{max}}} = \frac{DE_r}{QE_r} \tag{2}$$

where DE_{max} and QE_{max} are the detection efficiency and quantum efficiency of the reference point. The relative *CE* can be obtained by the relative *DE* (DE_r) divided by the relative *QE* (QE_r).

Fig.2. The 20-inch coated MCP-PMT sample developed in XIOPM.

A. Detection efficiency

In the photon counting mode, *DE* is defined as the ratio of the number of counted pulses (output pulses N_d) to the incident photons (N_p) [16]. Keeping the light intensity and time constant, N_p is supposed to be a constant for the tested PMTs. DE_r is given by

$$DE_r = \frac{DE}{DE_{max}} = \frac{\frac{N_d}{N_p}}{\frac{N_{dmax}}{N_p}} = \frac{N_d}{N_{dmax}} \tag{3}$$

N_{dmax} is the total number of the counted pulses in the single photoelectron (SPE) spectrum at the relative point.

The setup scheme to measure the SPE spectrum is shown in Fig.3. A dark box is built to house a 410 nm LED light source along with the PMT being tested. The LED employed in the tests is fired by a Tektronix AFG3102 pulse generator which outputs a TTL synchronization signal as well. By the TTL-to-NIM converter, the TTL synchronization signal is transformed to a NIM signal. The anode signal is sent to a CAEN V965 QDC which has two optional LSB (25 fC or 200 fC) to be digitized. For the high quality SPE spectrum measurements, the resolution of 25 fC is chosen. The transformed NIM signal serves as the integration trigger time window of QDC.

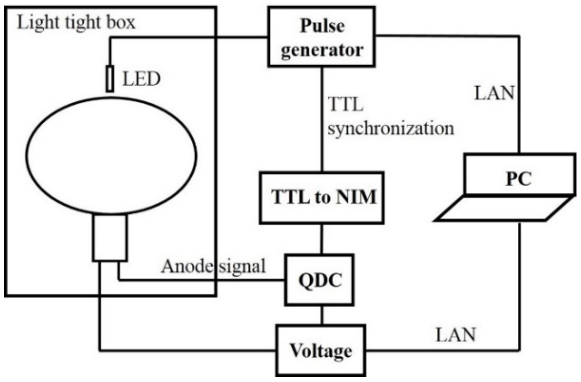

Fig.3. Schematic view of the SPE spectrum measurement setup.

The probability $P(n,\mu)$ that n photoelectrons (PEs) can be collected is expressed as

$$P(n,\mu) = \frac{\mu^n e^{-\mu}}{n!} \tag{4}$$

where μ is the mean number of photoelectrons emitted from the photocathode [17]. If the signal to pedestal (n = 0) ratio is 1/9 (it can be obtained by adjusting the light intensity), the probability of the single PE to that of the multiple PEs is $P(n = 1)/P(n > 1) = 21$. In this case, the signal is supposed to be SPE spectrum [18].

The SPE spectrums of the 20-inch typical and coated MCP-PMTs are measured. Several points in the angular range $-45° \le \theta \le 45°$, as exhibited in Fig.4. , are illuminated. Result in Fig.5. shows that the signal of the coated MCP-PMT (right side) has a narrower FWHM and higher peak, which indicates that the spread of the output pulse charge distribution is narrower, and the gain uniformity is better. Besides, energy resolution (also known as pulse height resolution, PHR) is expressed as

$$\mathrm{PHR} = \frac{\mathrm{FWHM}}{\mathrm{peak}} \times 100\ \% \tag{5}$$

Narrow signal FWHM and high peak will also result in a high precise PHR.

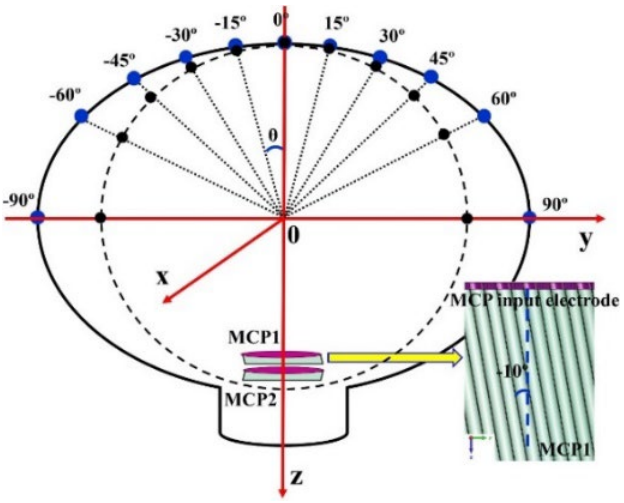

Fig.4. Diagrammatic sketch of the photocathode illuminated points represented by the blue dots and the included angle θ.

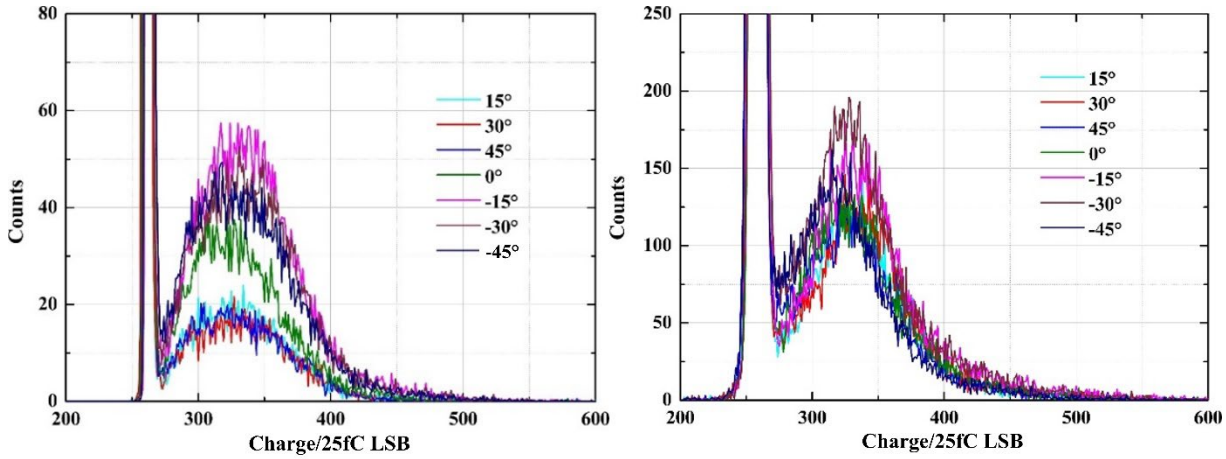

Fig.5. The typical (left side) and the coated (right side) MCP-PMT SPE spectrums for various illuminated points.

The point θ = -30° on the photocathode of the coated MCP-PMT is chosen as the reference for its maximum total number of the counted pulse. Fig.6. exhibits the relative detection efficiencies of the typical (DE_{rt}) and the coated (DE_{rc}) MCP-PMTs. As can be seen, DE_{rc} exceeds DE_{rt} substantially.

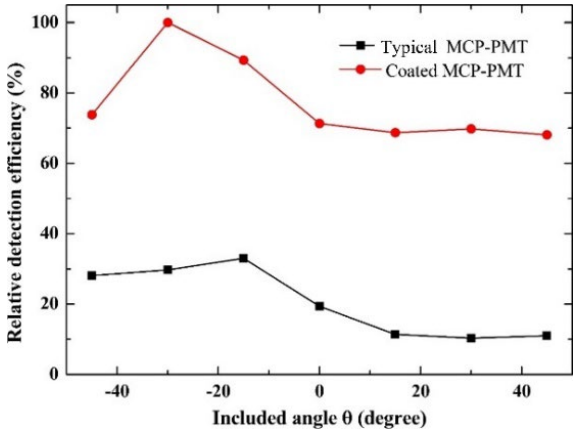

Fig.6. The relative detection efficiencies of the typical and the coated MCP-PMTs versus the illuminated position.

B. Quantum efficiency

QE is calculated by the following formula [19]:

$$QE = \frac{h \cdot c \cdot S}{\lambda \cdot e} \tag{6}$$

where h is Planck's constant, λ is the wavelength of the incident light, c is the light velocity in vacuum and e is the electron charge. S is the radiant sensitivity, namely,

$$S = \frac{I}{I_{light}} \tag{7}$$

I_{light} is the incident light intensity, which is kept constant. I is the cathode current of the MCP-PMT. QE_r is expressed as

$$QE_r = \frac{QE}{QE_{max}} = \frac{I}{I_{max}} \tag{8}$$

where I_{max} is the cathode current illuminated at the reference point.

A setup is built to measure the MCP-PMT cathode current. The 410 nm LED light is employed to illuminate the photocathode. The MCP-PMT photocurrents are measured by

a Keithley 6517B electrometer. Fig.7. shows the measured currents versus the applied voltage for the PMT samples at $\theta = 0°$. The current plateau indicates that all of the photoelectrons emitted from the cathode are collected, thus, the corresponding current value is adopted to calculate the relative *QE*. As exhibited in Fig.8., the relative quantum efficiencies of the typical and the coated MCP-PMTs peak at $\theta = -30°$ and -45°, respectively.

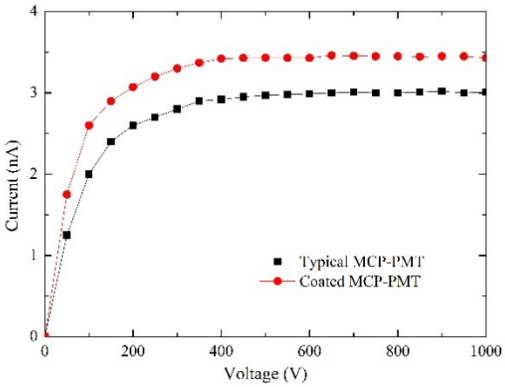

Fig.7. The measured cathode currents at 410 nm versus applied voltage for the PMT samples at $\theta = 0°$.

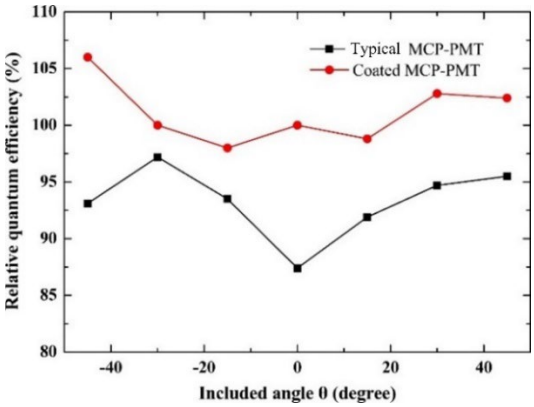

Fig.8. The relative quantum efficiencies of the typical and the coated MCP-PMTs versus the illuminated position.

C. Collection efficiency

Based on the above measurements, the relative collection efficiencies of the typical and the coated MCP-PMTs are obtained by (2). Results are exhibited in Fig.9. *CE* of the coated MCP-PMT has a significant improvement, which exceeds the typical one substantially over all the angular range. The collection efficiencies of the typical and the coated MCP-PMTs peak at $\theta = -15°$ and -30°, respectively. *CE* at the positive side is flatter. In addition, *CEs* of both typical and coated MCP-PMTs at the negative angles are higher than those at the positives with the same absolute value, which is attributed to the 10° bias angle of the MCP channel. Photoelectrons from the positive angles have a higher chance to land on the penetrating electrode layer than those at negatives with the same absolute value. Experiments validate that coating MCP with a high SEY film is an effective approach to improve *CE*. It is worth noting that uncertainties in Fig.6. to Fig.9. are small, and it is difficult to separate them from the data symbols.

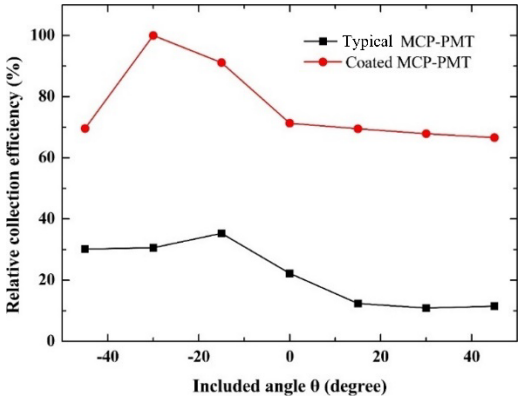

Fig.9. The relative collection efficiencies of the typical and the coated MCP-PMTs versus the illuminated position.

3. CONCLUSIONS

Coating MCP with a high SEY material is supposed to be an effective approach to improve *CE* of the large area MCP-PMT. In this work, experiments are conducted to validate its feasibility and effectiveness. A relative method is developed to characterize the *CE* performance. Results show that *CE* of the coated MCP-PMT has a significant improvement. This research gives an important reference for the development of the detectors based on the MCP with high *CE*, *DE* and high precise PHR requirements.

ACKNOWLEDGMENT

This study is supported by the National Natural Science Foundation of China (Grant No. 12005083) and the Ph.D. Project supported by the Jinling Institute of Technology (Grant No. jit-b-201837).

REFERENCES

[1] Brugière, T. (2017). The Jiangmen underground neutrino observatory experiment. *Nuclear Instruments and Methods in Physics Research Section A: Accelerators, Spectrometers, Detectors and Associated Equipment*, 845, 326-329. https://doi.org/10.1016/j.nima.2016.05.111

[2] Li, Y. (2014). Overview of the Jiangmen underground neutrino observatory (JUNO). *International Journal of Modern Physics: Conference Series*, 31, 1460300. https://doi.org/10.1142/S2010194514603007

[3] He, M., JUNO collaboration. (2015). Jiangmen underground neutrino observatory. *Nuclear and Particle Physics Proceedings*, 265-266, 111-113. https://doi.org/10.1016/j.nuclphysbps.2015.06.027

[4] Zhang, Y., Hui, J., Liu, J., Xiao, M., Zhang, T., Zhang, F., Meng, Y., Xu, D., Ye, Z. (2021). Cable loop calibration system for Jiangmen underground neutrino observatory. *Nuclear Instruments and Methods in Physics Research Section A: Accelerators, Spectrometers, Detectors and Associated Equipment*, 988, 164867. https://doi.org/10.1016/j.nima.2020.164867

[5] Miramonti, L. (2020). Status and the perspectives of the Jiangmen Underground Neutrino Observatory (JUNO). *Modern Physics Letters A*, 35 (09), 2030004. https://doi.org/10.1142/S0217732320300049

[6] Cerna, C. (2020). The Jiangmen Underground Neutrino Observatory (JUNO). *Nuclear Instruments and Methods in Physics Research Section A: Accelerators, Spectrometers, Detectors and Associated Equipment*, 958, 162183. https://doi.org/10.1016/j.nima.2019.05.024

[7] Leitner, R. (2017). Recent results of Daya Bay reactor neutrino experiment. *Nuclear and Particle Physics Proceedings*, 285-286, 32-37. https://doi.org/10.1016/j.nuclphysbps.2017.03.007

[8] An, F., Bai, J., Balantekin, A., et al. (2012). Observation of electron-antineutrino disappearance at Daya Bay. *Physical Review Letters*, 108, 171803. https://doi.org/10.1103/PhysRevLett.108.171803

[9] Cao, J. (2014). Daya Bay and Jiangmen underground neutrino observatory (JUNO) neutrino experiments. *Scientia Sinica Physica, Mechanica & Astronomica*, 44 (10), 1025-1040. https://doi.org/10.1360/SSPMA2014-00174

[10] Wang, Y., Qian, S., Zhao, T., et al. (2012). A new design of large area MCP-PMT for the next generation neutrino experiment. *Nuclear Instruments and Methods in Physics Research Section A: Accelerators, Spectrometers, Detectors and Associated Equipment*, 695, 113-117. https://doi.org/10.1016/j.nima.2011.12.085

[11] Qian, S., Liu, S. (2016). The R&D of 20 inch MCP-PMTs in China. In *38th International Conference on High Energy Physics*. http://indico.cern.ch/event/432527/contributions/1071941/

[12] Hamamatsu Photonics K.K. (2006). *Photomultiplier Tubes: Basics and Applications*. Third edition.

[13] Bronshtein, I., Denisov, S. (1967). Secondary electron emission of aluminium and nickel for obliquely incident primary electrons. *Soviet Physics-Solid State*, 9, 731-732.

[14] Chen, L., Tian, J., Liu, C., et al. (2016). Optimization of the electron collection efficiency of a large area MCP-PMT for the JUNO experiment. *Nuclear Instruments and Methods in Physics Research Section A: Accelerators, Spectrometers, Detectors and Associated Equipment*, 827, 124-130. https://doi.org/10.1016/j.nima.2016.04.100

[15] Chen, L., Tian, J., Zhao, T., Liu, C., Liu, H., Wei, Y., Sai, X., Chen, P., Wang, X., Lu, Y., Hui, D. (2016). Simulation of the electron collection efficiency of a PMT based on the MCP coated with high secondary yield material. *Nuclear Instruments and Methods in Physics Research Section A: Accelerators, Spectrometers, Detectors and Associated Equipment*, 835, 94-98. https://doi.org/10.1016/j.nima.2016.08.034

[16] CST Studio Suite. (2014). *Computer Simulation Technology*. https://www.cst.com

[17] Chirikov-Zorin, I., Fedorko, I., Menzione, A., Pikna, M., Sýkora, I., Tokár, S. (2001). Method for precise analysis of the metal package photomultiplier single photoelectron spectra. *Nuclear Instruments and Methods in Physics Research Section A: Accelerators, Spectrometers, Detectors and Associated Equipment*, 456 (3), 310-324. https://doi.org/10.1016/S0168-9002(00)00593-3

[18] Xia, J., Qian, S., Wang, W., et al. (2015). A performance evaluation system for photomultiplier tubes. *Journal of Instrumentation*, 10, 03023. https://doi.org/10.1088/1748-0221/10/03/P03023

Received March 11, 2022
Accepted June 27, 2022